Ceramics International 44 (2018) 21004–21014

Contents lists available at ScienceDirect

Ceramics International

journal homepage: www.elsevier.com/locate/ceramint

Physicochemical, osteogenic and corrosion properties of bio-functionalized ZnO thin films: Potential material for biomedical applications

Luciana D. Trino[a,*], Luiz G.S. Albano[a], Erika S. Bronze-Uhle[a], Anne George[b], Mathew T. Mathew[c], Paulo N. Lisboa-Filho[a]

[a] São Paulo State University (Unesp), School of Sciences, Bauru, SP 17033-360, Brazil
[b] Department of Oral Biology College of Dentistry, University of Illinois at Chicago, Chicago, IL, 60612, USA
[c] Department of Biomedical Sciences, College of Medicine at Rockford, University of Illinois-School of Medicine at Rockford, Rockford, IL, 61107-1897, USA

ARTICLE INFO

Keywords:
Zinc oxide
Bio-functionalization
Osteogenic peptides
Corrosion resistance
Functional materials

ABSTRACT

Nano-sized zinc oxide (ZnO) is well known for its antibacterial activity and biocompatibility, which make this material a promising candidate to tailor titanium (Ti) implant surfaces. In an optimized scenario, the antibacterial activity of ZnO and its biocompatibility can be envisioned as a good bio-functionalization strategy to increase osteointegration. Thus, in this work, it is proposed that the bio-functionalization of ZnO thin films with dentin matrix protein 1 (DMP1) peptides could function as an apatite crystal nucleator. Ti was coated with ZnO and functionalized with two different spacers, 3-(4-aminophenyl) propionic acid (APPA) or 3-mercaptopropionic acid (MPA) to facilitate binding with DMP1 peptides. Attenuated total reflection Fourier transform infrared (ATR-FTIR) spectroscopy and X-ray photoelectron spectroscopy (XPS) results confirmed the presence of the peptides on the ZnO thin film surface through characteristic bands related to amine and carboxylic acid groups and by the incidence of N 1 s spectra, respectively. Atomic force microscopy (AFM) images indicated that a more uniform layer of DMP1 peptides is formed in the the presence of the APPA and MPA spacers. In general, the results obtained showed that the bio-functionalized ZnO thin films with APPA spacer, ZnO APPA P sample, presented enhanced wettability (17°), surface energy (72 dyn/cm), with an osteogenic surface and apatite nucleating properties. Furthermore, the electrochemical analysis showed increased corrosion resistance with noble E_{OCP} (−0.13 V), Ecorr (−0.46 V), and Icorr (8.91×10^{-7} A/cm^2) values. These findings indicated promising applications of ZnO APPA P in biomedical devices once it can accelerate the osteointegration process and improve the corrosion resistance of implants.

1. Introduction

The major causes of titanium dental implant failures are related to inadequate implant-to-bone contact, implant degradation and bacterial infection [1,2]. Some physicochemical surface modification procedures have been used to minimize these effects, such as surface coatings [3], chemical grafting [4], and ions or biomolecules incorporation [5] on the implant surface. Furthermore, to overcome this issue, osteogenic biomolecules in combination with bactericide agents can be incorporated onto titanium surface to improve implant osteointegration, corrosion resistance and prevent infections associated with implantation processes [6].

Nano-sized zinc oxide (ZnO) is well known for its significant antibacterial activity over a wide spectrum of bacterial species [7]. Interestingly, ZnO is non-toxic, presenting good biocompatibility to human cells [8]. Zinc ions have been considered essential elements to promote bone formation through the stimulation, proliferation, adhesion, and differentiation of osteoblasts [9]. In addition, several studies reported its outstanding corrosion resistance [10–13]. Therefore, ZnO deposition on implant surfaces may improve or induce the osseointegration process with considerable corrosion resistance.

ZnO can be deposited on titanium surfaces by low-cost methods for large-scale manufacturing. For example, ZnO can be synthesized from sol-gel precursors and deposited by spin coating method [10]. In addition, the functionalization of metal oxides with self-assembled monolayers (SAMs) can be used to manipulate its surface physicochemical properties, such as roughness, wettability, and surface energy. These properties directly affect protein adsorption, cell adhesion, proliferation and osteoblastic differentiation [14]. In this way, the functionalization of metal oxides with self-assembled monolayers (SAMs) to

* Corresponding author.
E-mail address: lucianatrino@fc.unesp.br (L.D. Trino).

https://doi.org/10.1016/j.ceramint.2018.08.136
Received 19 June 2018; Received in revised form 11 August 2018; Accepted 11 August 2018
Available online 13 August 2018

immobilize biomolecules, e.g. proteins, peptides, growth factors, may result in a surface with higher bioactivity.

Dentin matrix protein 1 (DMP1) peptides, related to osteoblast/odontoblast differentiation, are known to act as nucleators for hydroxyapatite formation [15]. More specifically, the peptides ESQES and QESQSEQDS derived from DMP1 can induce the formation of plate-shaped apatite crystals [16]. The molecular mechanism is associated with the stabilization of calcium ions due to the presence of acidic groups on DMP1 peptides, e.g., glutamic acid, aspartic acid, and serine [17]. Consequently, the DMP1 peptides can play a vital role in controlled mineral deposition.

The focus of the present study is based on the bio-functionalization of the ZnO thin films with DMP1 peptides covalently immobilized through 3-(4-aminophenyl) propionic acid (APPA) or 3-mercaptopropionic acid (MPA) SAMs. Therefore, the physicochemical characteristics of the modified ZnO thin films are presented here. Mineralization and corrosion resistance properties of the bio-functionalized ZnO thin films were also evaluated. Furthermore, human mesenchymal stem cells (hMSCs) adhesion, proliferation, and differentiation upon the modified surfaces were also discussed in detail.

2. Materials and methods

2.1. Materials

All materials utilized for ZnO thin film fabrication were reagent grade and deionized water was used as a solvent. Zinc oxide (ZnO), citric acid ($HOC(COOH)(CH_2COOH)_2$), ethylene glycol ($C_2H_4(OH)_2$), hydrogen peroxide (H_2O_2), 3-mercaptopropionic acid ($HSCH_2CH_2CO_2H$), 3–4 aminophenyl propionic acid ($H_2NC_6H_4CH_2CH_2CO_2H$), phosphate buffered saline solution, formalin, ascorbic acid ($C_6H_8O_6$), β-glycerophosphate disodium ($(HOCH_2)_2CHOP(O)(ONa)_2$), and sodium phosphate (Na_3PO_4) were the products of Sigma-Aldrich (USA). Nitric acid (HNO_3), sulfuric acid (H_2SO_4), hydrochloric acid (HCl), and ethanol (CH_3CH_2OH) were purchased from Merck (USA). The materials for cell culture, including minimum essential medium Eagle (α-MEM), fetal bovine serum (FBS), L-glutamine, and antibiotic-antimycotic cocktail were the products of Gibco (USA). The CellTiter 96® AQueous One Solution Cell Proliferation Assay, or MTS reagent, was purchased from Promega (USA). All the reagents for PCR assay were purchased from Qiagen (USA), including RNeasy® kit membrane and the genes: alkaline phosphatase (ALP), osteopontin (OPN), osteocalcin (OCN), runt-related transcription factor 2 (Runx2), bone sialoprotein (BSP), alpha-1 type-1 collagen (Col1a1), and glyceraldehyde-3-phosphate dehydrogenase (GAPDH).

2.2. Dentin matrix protein 1(DMP1) peptides deposition

Commercial pure titanium grade 4 (Ti cp4 (ACNIS, Brazil)) discs, with a diameter of 12.7 mm and 3 mm of thickness, were prepared and coated with ZnO based in our previous work [10]. Briefly, the ZnO resin was synthesized by sol-gel method dissolving 72.05 g of citric acid in 200 mL of deionized water. Subsequently, 15.00 mL of nitric acid was added to the mixture with 10.17 g of zinc oxide. A molar ratio of 1:3 was maintained between ZnO and citric acid, respectively. The solution was then heated to 100 °C for 15 min. Finally, ethylene glycol was added to the solution considering a mass ratio between the citric acid and ethylene glycol of 60:40, respectively. Following, the temperature was increased to 150 °C and the solution kept under magnetic stirring until reach 100 mL. Then, the solution was diluted to a ratio of 5 mL of deionized water to 3 mL of ZnO resin. After the Ti discs were sand-blasted and etched with Piranha solution (a mixture of 7:3 (v/v) 98% H_2SO_4 and 30% H_2O_2) the diluted ZnO solution was deposited by spin coating technique (2000 rpm during 60 s) [10]. Then, the ZnO surface was functionalized with two different bifunctional molecules 3-mercaptopropionic acid (MPA) and 3–4 aminophenyl propionic acid (APPA) by immersion method [10]. The 2 mM APPA solution was prepared in ethanol absolute by stirring until complete dissolution. Then it was heated to 40 °C and the samples were immersed for 5 min [10]. An aqueous MPA solution (1 mM) was prepared by adjusting the pH to 3 with HCl. Then, the samples were immersed for 10 min in the MPA solution [10]. After the deposition of the organic molecules, all samples were dried in ambient conditions and kept in a desiccator until use.

Peptides pA (ESQES) and pB (QESQSEQDS) derived from DMP1 were synthesized via solid phase. The peptides were diluted in the ratio 1 of pA to 4 of pB in carbonate buffer solution to have a final concentration of 1 mg/mL. The deposition was performed following the literature [18]. In order to perform the crosslink between the peptides over the samples, they were maintained immersed in peptides solution overnight under UV-light in a biological safety cabinet.

The peptides adhesion was analyzed by X-ray photoelectron spectroscopy (XPS, Scienta Omicron ESCA), and attenuated total reflection Fourier transform infrared (ATR-FTIR) spectroscopy (Bruker Vertex 70). The contact angle and surface energy were evaluated by the sessile drop technique in a goniometer (Ramé-Hart, 100-00) employing deionized water (polar substance) and diiodomethane (non-polar substance) as the probing liquids. Atomic force microscopy (AFM, Park Systems) was used to analyze the topography of the samples in non-contact mode.

2.3. Biocompatibility and cell proliferation studies

2.3.1. Cell culture

Human mesenchymal stem cells containing the gene for Green Fluorescence Protein (GFP) were seeded upon the samples into 24-well plates at a density of 2×10^4 per well. The cells were kept in an incubator at 37 °C and 5% of CO_2 concentration for 24 h and 7 days, until reach confluence. Fresh culture medium was changed every other day. The complete media was prepared with minimum essential medium–alpha (α-MEM), 20% of fetal bovine serum (FBS), 1% L-glutamine and 1% antibiotic-antimycotic cocktail.

2.3.2. Cell adhesion and viability assay

The adhesion of hMSCs upon the substrates was analyzed by confocal fluorescence microscopy (Zeiss, LSM 710) in triplicates using a 20× lens. The protocol used consists of culturing the cells per 24 h and 7 days, then they were fixed with buffered neutral formalin 10%. The images from 24 h of cell culture did not present significant changes (Fig. S6).

The cells were also characterized by a colorimetric method to determine the number of viable cells in proliferation. This method is based on the reduction of MTS reagent ((3-(4,5-dimethylthiazol-2-yl)-5-(3-carboxymethoxyphenyl)-2-(4-sulfophenyl)-2H-tetrazolium)) by viable cells to generate formazan products that are directly soluble in cell culture medium. The absorbance of the formazan product is an indicator of metabolically active mitochondria from viable cells, thus it is an indirect method to determine cell viability. In this way, the assay was performed using a CellTiter 96® AQueous One Solution Cell Proliferation Assay (PROMEGA) kit. The cells were cultured for 1, 3 and 5 days in triplicates. To measure the amount of soluble formazan produced by cellular reduction of MTS, 20 μL of CellTiter 96® AQueous One Solution reagent was pipetted into each well containing the samples in 100 μL of culture medium. The plates were incubated at 37 °C for 1 h in a humidified, 5% CO_2 atmosphere. Finally, the plates were read in a Synergy 2 multi-mode plate reader at 490 nm. The quantity of formazan product measured by absorbance at 490 nm was directly proportional to the number of living cells in culture.

2.3.3. Cell differentiation by quantitative real-time polymerase chain reaction (RT-PCR)

Human mesenchymal stem cells were cultured during 7 days upon

the samples in a 2.5×10^4 cell concentration per well. Two sets of samples were analyzed in triplicates from each group. A positive control group was analyzed in a polystyrene surface. In the first one hMSCs were cultured with an osteogenic induction media containing 50 mg/mL ascorbic acid and 10 mM β-glycerophosphate disodium; in the second hMSCs were cultured with a standard media, as a control. Total RNA was isolated from hMSCs using RNeasy kit membrane (Qiagen) by spin technology according to the manufacturer's instructions. The cells were disrupted in a lysis buffer and homogenized. Ethanol was then added to the lysate, creating conditions that promote selective binding of RNA to the RNeasy kit membrane. The sample was then applied to the RNeasy Mini spin column. Total RNA binds to the membrane, contaminants were efficiently washed away, and high-quality RNA was eluted in RNase-free water. All bind, wash, and elution steps were performed by centrifugation in a microcentrifuge [19]. The solutions were placed in a 96 well plate to be read in a real-time PCR Reader (StepOnePlus, Applied Biosystems). The genes of interest included alkaline phosphatase (ALP), alpha-1 type-1 collagen (Col1a1), osteopontin (OPN), osteocalcin (OCN), runt-related transcription factor 2 (Runx2), and bone sialoprotein (BSP). Glyceraldehyde-3-phosphate dehydrogenase (GAPDH) was used as an internal control.

2.4. In vitro mineralization assay

Nucleation was carried out under high concentrations of calcium and phosphate following a previously described protocol [19]. Briefly, the samples were immersed in a 1 M of calcium chloride solution during a period of 30 min, washed extensively in water, and then immersed in a 1 M of sodium phosphate solution for a period of 30 min. Finally, they were washed with water and dehydrated from 20% to 100% of ethanol solution and then dried with hexamethyldisilazane (HMDS). The samples were then analyzed by scanning electron microscopy with energy dispersive spectroscopy (SEM/EDS) (Zeiss, EVO LS15) in triplicate.

2.5. Electrochemical measurements

Electrochemical tests were conducted with a Metrohm Autolab PGSTAT302 equipped with a FRA32M module using a standard three-electrode corrosion cell. Samples were considered as the working electrode with about 1 cm^2 of the exposed surface area to corrode. The other two electrodes were a platinum wire as a counter and an Ag/AgCl as a reference electrode (Metrohm). A quantity of 40 mL of PBS was used for each sample as the electrolyte. All tests were performed at the physiological temperature of 37 °C using a hot plate. Each group was analyzed in triplicate. The electrochemical protocol based in our previous work [10] consisted of an initial open circuit potential (OCP), a second OCP, an electrochemical impedance spectroscopy (EIS), a potentiodynamic polarization (PD), and a final OCP. The second OCP was performed during 3600 s to allow the samples to stabilize in the specific conditions of the electrochemical cell. The EIS was performed to analyze Bode and Phase Angle plots, in order to obtain the specific features from the interface through an equivalent circuit approach. EIS measurement was performed at the second open circuit potential (E_{OCP}) with a potential amplitude of ± 10 mV and frequency range between 100 kHz and 0.01 Hz. Finally, PD was used to determine the corrosion potential (E_{corr}) and corrosion current density (I_{corr}) using Tafel extrapolation [7]. PD was performed by a cyclic polarization between − 0.8 V and + 1.8 V.

2.6. Statistical analysis

Each experiment was performed at least three times and the results are expressed as a mean ± standard deviation for each experiment.

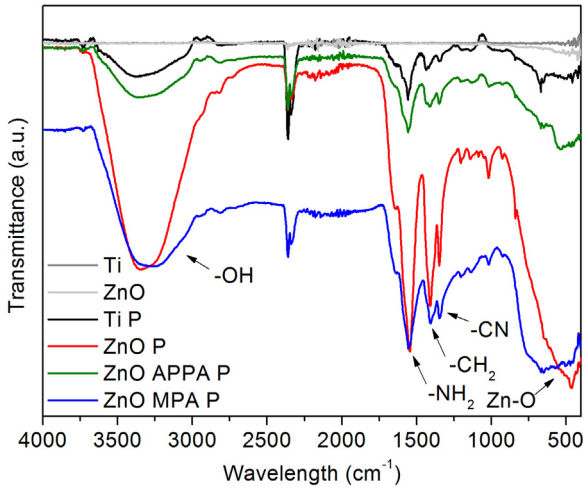

Fig. 1. ATR-FTIR spectra for the control (Ti and ZnO) and bio-functionalized surfaces (Ti P, ZnO P, ZnO APPA P, and ZnO MPA P, where P is related to the DMP1 peptides). The presence of the peptides on the Ti P, ZnO P, ZnO APPA P, and ZnO MPA P surface was evidenced by -NH_2 and C-N groups at 1536 cm^{-1} and 1337 cm^{-1}, respectively.

3. Results and discussion

3.1. Bio-functionalization of ZnO thin films

The bio-functionalization of the samples with the peptides derived from DMP1 was confirmed by ATR-FTIR, as shown in Fig. 1. After the bio-functionalization, characteristic bands related to amine and carboxylic acid groups from the DMP1 peptides could be detected for all samples at 1337 cm^{-1}, 1408 cm^{-1}, 1536 cm^{-1} and 3340 cm^{-1}. The broadband at 3340 cm^{-1} was assigned to the stretching of hydroxyl groups (–OH) [20]. Bands at 1536 cm^{-1} and 1337 cm^{-1} were related to amine groups (–NH_2) and C–N bonds [21], respectively. The vibration at 1536 cm^{-1} was attributed to -NH_2 deformation and was considered indicative of peptides or amino acids [22]. The band at 1408 cm^{-1} was characteristic of the –CH_2 bonds [23]. Furthermore, the stretching mode of the Zn–O bond could be seen in the range from 540 to 570 cm^{-1} [24].

XPS results indicated the presence of elements Zn, O, Ti, C and N, Fig. 2a. In addition, it was possible to observe the contribution of elements such as Na 1s, Cl 2p and P 2p in the survey spectra originated from the PBS solution, used to dilute the peptides. Furthermore, no adventitious nitrogen was detected on the surface of the Ti and ZnO control samples, thus the presence of the N 1s spectra was an evidence of the peptides bio-functionalized on the ZnO thin film surface.

In the N 1s spectra two contributions were observed as shown in Fig. 2b. The main component (N1) was centered between 399.5.5 eV and 400.1 eV, related to the amide groups in the peptide backbones and amine groups on the side chains [25]. Furthermore, this value was in the range for protonated nitrogen (NH_3^+), being an indication of the zwitterionic protonated α-amine nitrogen present in the serine, glutamine, aspartic, and glutamic acid structures [26]. The component at lower binding energy (N2) around 397.4–398.5 eV was consistent with amide groups that were strongly interacting with inorganic substrates [27]. The increased area of the N2 component for the samples ZnO APPA P and ZnO MPA P may be an indication of higher affinity between the peptides and the ZnO thin film surface due to the presence of the bifunctional organic molecules (APPA and MPA). In our previous study, it was reported that APPA and MPA molecules adhered to the ZnO thin film surface through carboxylic acid and thiol groups [10], respectively. These types of interaction led to free terminal amine (-NH_2) and carboxylic acid groups (-COOH) on the surface, which could interact with the acidic and amino groups from the peptides. Considering that a

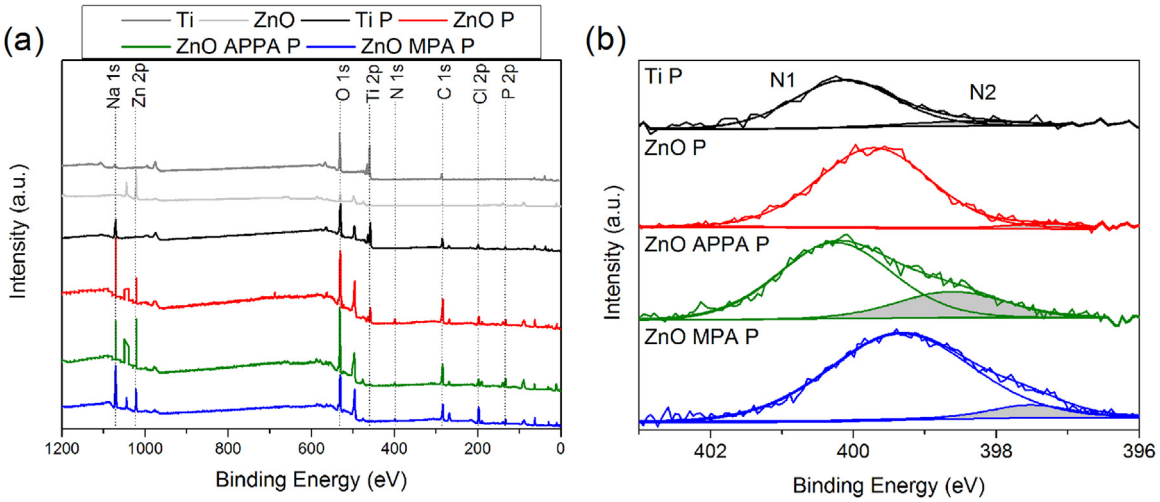

Fig. 2. XPS survey spectra (a) for the control (Ti and ZnO) and bio-functionalized surfaces (Ti P, ZnO P, ZnO APPA P, and ZnO MPA P). The presence of DMP1 peptides was indicated by the C 1s, O 1s, and N 1s peaks at the survey spectra. N 1 s high-resolution spectra (b) for the bio-functionalized surfaces. Further, N 1s spectra showed two contributions: the main component (N1) related to amide groups in the peptide backbones and amine groups on the side chains; and an N2 component consistent with amide groups that were strongly interacting with inorganic substrates.

strong interaction, higher affinity is expected to improve the DMP1 peptides adhesion. More detailed XPS data can be found in Fig. S1-S4 from Supporting information.

Water contact angle and surface energy analysis were also investigated to evaluate the physicochemical properties of the bio-functionalized surfaces. The water contact angle values are shown in Fig. 3a. The pristine Ti surface showed a water contact angle of 72°. After the ZnO thin film deposition, an increase in water contact angle to 81° was observed, indicating a more accentuated hydrophobic behavior than Ti. This decrease in the wettability can be associated with the surface morphology effect in which the air interfaces or grooves between the individual structures can affect the contact angle [28]. In addition, as can be seen in Fig. 3a, the bio-functionalization with the peptides resulted in significant changes in the water contact angles for all the samples. The surfaces modified with the DMP1 peptides showed a similar hydrophilicity with water contact angles between 13° and 20°, with no significant differences between the samples. This increased wettability can be correlated with the charged peptides on the surface [29]. The isoelectric point (pI) for peptides pA and pB is 3.52 and 3.41, respectively [18]. In higher pH values, such as the pH 9.2 from carbonate buffer solution (used for deposition), the peptides are negatively charged. Specifically, at the deposition pH value, the overall charge density for peptides pA and pB are respectively −3 and −4 [18], thus improving the hydrophilicity. The surface energy was inversely proportional to water contact angle, showing elevated values (around 72 dyn/cm) for the samples bio-functionalized with the DMP1 peptides, Fig. 3b. This increase can also be related with the overall charge density for peptides pA and pB. Therefore, the variations in wettability and surface energy confirmed the process of bio-functionalization.

The surface topography of the bio-functionalized samples was analyzed by AFM considering an area of 1 μm x 1 μm, Fig. 4. Considering Ti P (Fig. 4b) and ZnO P (Fig. 4d) the results indicated that the peptides formed agglomerated structures in isolated regions as compared with the controls Ti (Fig. 4a) and ZnO (Fig. 4c). Furthermore, because of the non-homogeneous coverage of the Ti surface, it was not possible to observe the peptides on the Ti P sample, only the Ti grains were visible in Fig. 4b. A topography considering a higher area is shown in Fig. S5 for Ti P sample. The formation of peptides agglomerates may be due to the cooperative effects between the peptides, in which the adsorbed peptides increase the adsorption of others in solution [30]. On the other hand, a more uniform layer was formed by the presence of the APPA and MPA spacers (Fig. 4e-f). In ZnO APPA P and ZnO MPA P

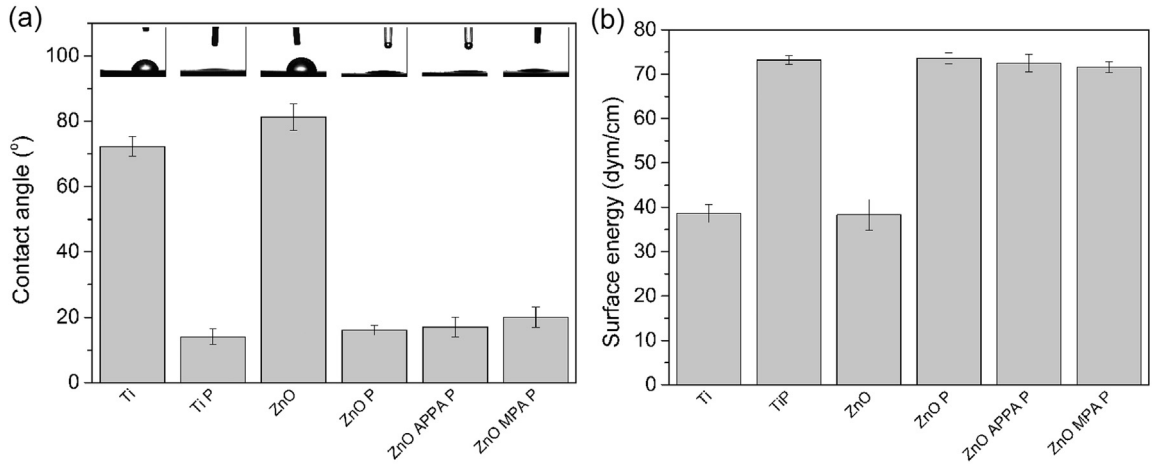

Fig. 3. Change in the water contact angles (a) and surface energy (b) for the control and bio-functionalized surfaces. It is evident that the presence of DMP1 peptides on ZnO thin film surfaces increased the hydrophilicity and surface energy of the materials, which are related with their overall charge density (pA = −3 and pB = −4).

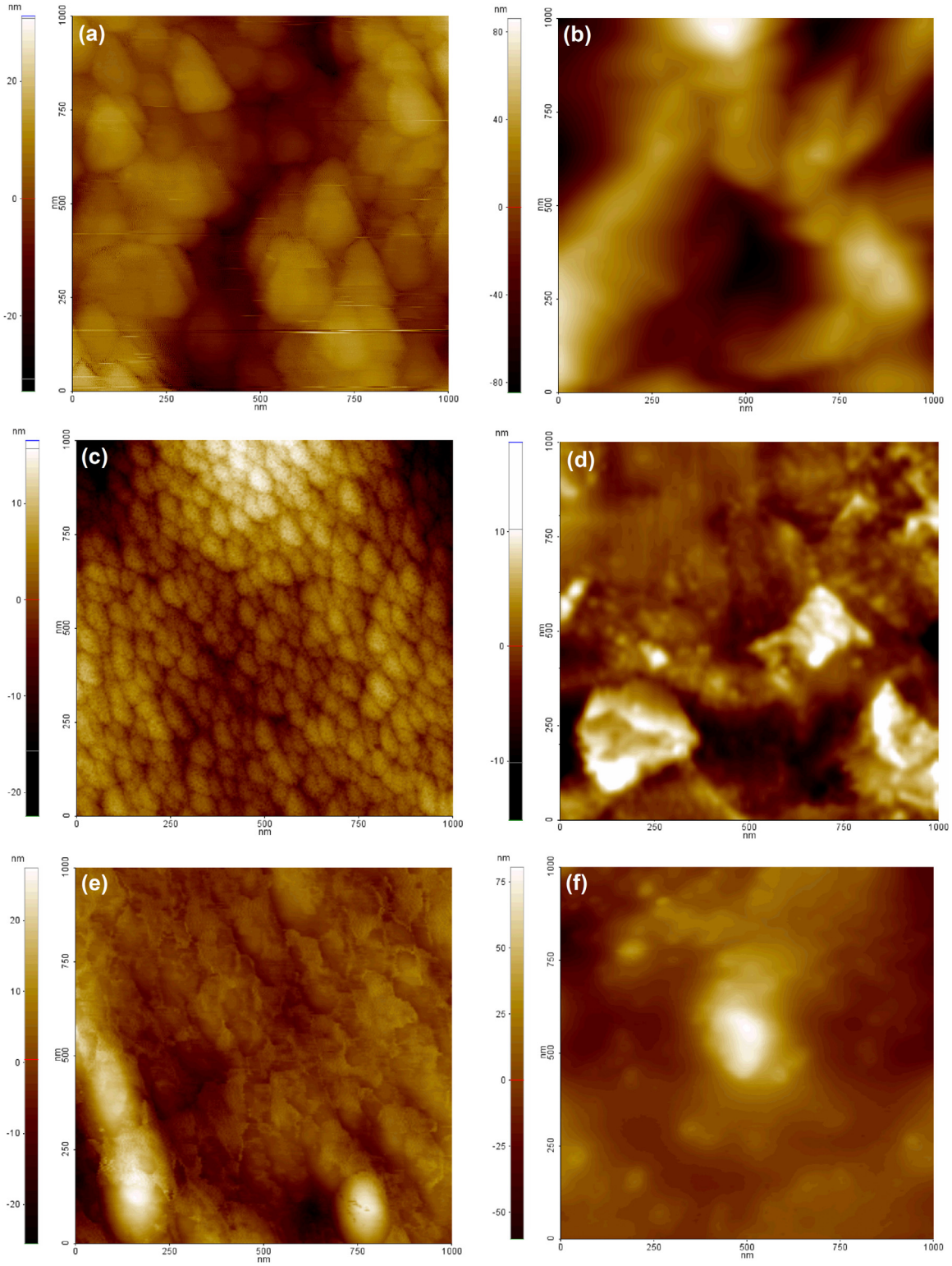

Fig. 4. AFM images for the different analyzed surfaces: Ti (a), Ti P (b), ZnO (c), ZnO P (d), ZnO APPA P (e), and ZnO MPA P (f). The control samples (Ti and ZnO) formed agglomerated peptides structures, while a more uniform dense layer of DMP1 peptides was formed with the presence of the APPA and MPA spacers due to the presence of -NH_2 and -COOH groups.

samples, the peptides appeared to be homogeneously distributed on the surface due to the presence of the terminal functional groups -NH_2 and -COOH, which have bound respectively to the carboxylic acid and amino groups of the peptides.

Additionally, the arithmetic surface roughness (Ra) was analyzed by AFM and also suggested an inhomogeneous surface coverage for Ti P. An increase in surface roughness from 6.0 (± 1.3) nm for Ti to 15.0 (± 3.3) nm for Ti P sample was observed. The average Ra values showed no significant difference for the bio-functionalized ZnO thin films, with an increase in the following sequence: ZnO < ZnO P < ZnO APPA P < ZnO MPA P, as indicated by the respectively values 2.9 (± 1.1) nm, 4.2 (± 1.4) nm, 5.4 (± 1.3) nm, and 7.9

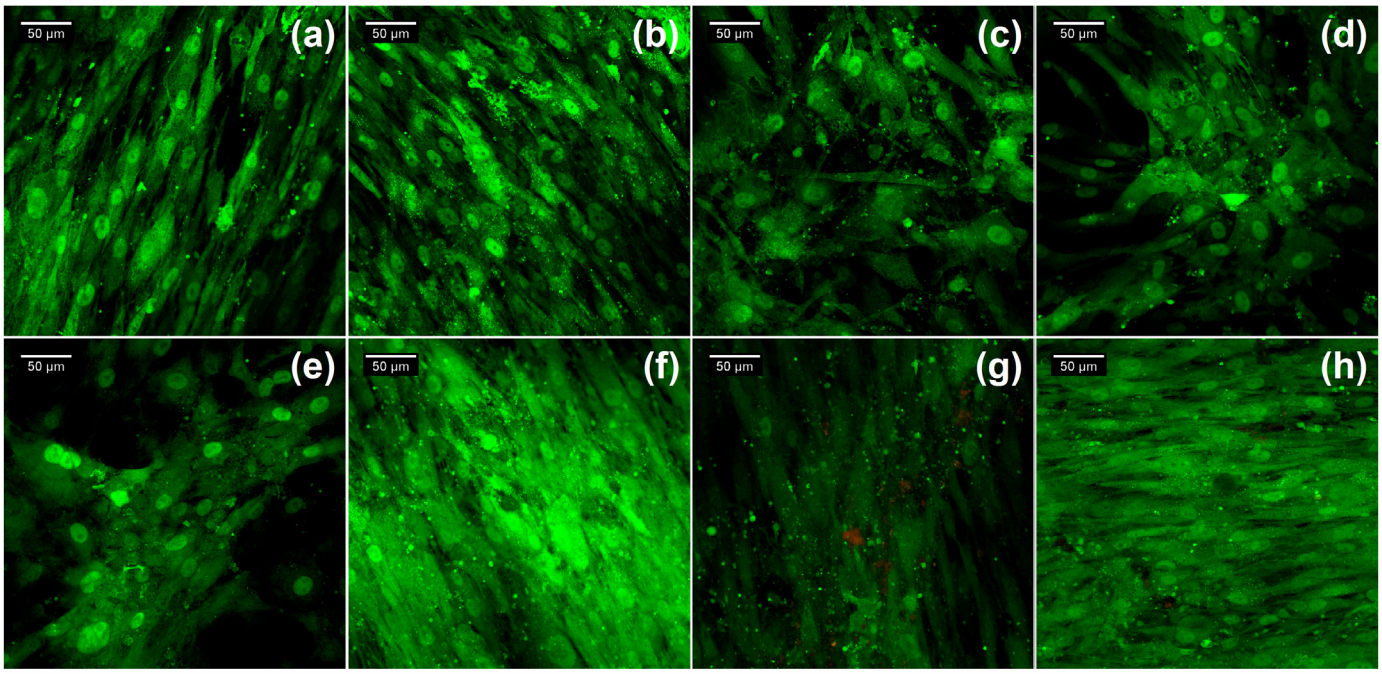

Fig. 5. Human mesenchymal stem cells labeled with green fluorescence protein visualized by confocal fluorescence microscope in day 7 at different substrates: Ti (a), Ti P (b), ZnO (c), ZnO P (d), ZnO APPA (e), ZnO APPA P (f), ZnO MPA (g) and ZnO MPA P (h). The presence of the peptides increased cell adhesion and proliferation, specifically for ZnO APPA P and ZnO MPA P samples.

(± 2.7) nm.

3.2. Adhesion and proliferation assay of human mesenchymal stem cells

The adhesion of hMSCs after 7 days in culture was characterized by fluorescence confocal microscopy as an indication of cell attachment, proliferation, and the start of the differentiation cascade. Fig. 5. revealed that the cells adopted an elongated shape and were well spread out, exhibiting a polarized morphology for the different samples. More specifically, an increased adhesion and growth were observed for the bio-functionalized samples. Cells can recognize stimuli from the underlying surface and convert these stimuli into specific intracellular signals to properly respond to changes in their surroundings [31]. The biochemical properties, stiffness, and topography of the extracellular matrix transduce signals into the interior of cells, which regulate cell differentiation, cell cycle, cell migration, and cell survival [32]. In this way, the modification in the physicochemical properties of ZnO thin films surfaces, caused by the presence of the DMP1 peptides, indicated that the peptides can modulate cell affinity and possibly the differentiation. Interestingly, ZnO thin films with organic molecules and peptides exhibited dots with a red fluorescence. This effect can be associated with the conjugation of ZnO nanostructures with organic molecules [33]. ZnO exhibits efficient emission in the region of blue, near UV, and may also exhibit luminescence in the green region related to oxygen vacancies [33].

A preliminary in vitro viability assay (MTS) performed at one, three and five-day intervals investigated hMSCs proliferation, Fig. 6. MTS is a sensitive assay to assess osteoblast proliferation because of its capability to measure indirectly the cell viability through the approximate determination of mitochondrial dehydrogenase activity [34]. The results showed that in general, the cell proliferation rate was higher in the bio-functionalized samples. In addition, no significant cytotoxicity was observed. However, mitochondrial activity is a key regulatory mechanism of the differentiation process of stem cells [35]. During differentiation, osteoblasts may decrease mitochondrial activity [36]. In this way we suggest that, in these experimental conditions, the ZnO APPA P sample might be interfering in differentiation events of these cells, decreasing the mitochondrial dehydrogenase activity. Thus, further investigations on the osteogenic differentiation are presented.

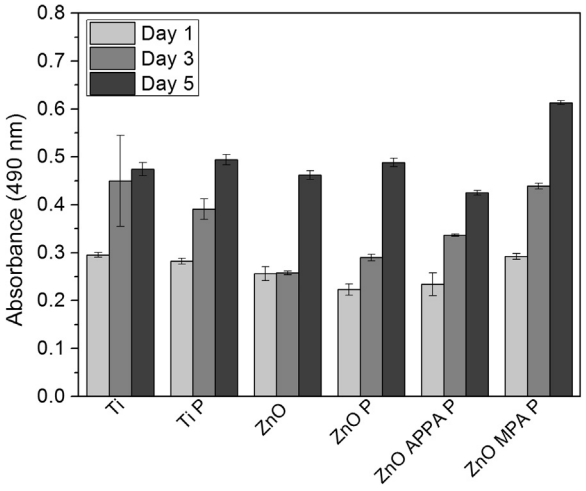

Fig. 6. Cell viability assay using MTS tetrazolium salt. The assay was performed with human mesenchymal stem cells cultured on the top of the controls (Ti and ZnO) and the bio-functionalized ZnO thin film surfaces for 1, 3 and 5 days.

3.3. Osteogenic differentiation of hMSCs in vitro

To further evaluate hMSCs differentiation at the molecular level, the expression of ALP, OCN, OPN, Col1a1, BSP, and Runx2 genes were quantified via real-time PCR (RT-PCR), on the pure Ti, ZnO, and bio-functionalized surfaces after culturing for 7 days, Fig. 7. In general, the presence of the DMP1 peptides increased the expression of the genes, with exception of ZnO MPA P sample. Furthermore, a positive control (polystyrene surface) was analyzed and showed that for most genes the bio-functionalized ZnO thin film surfaces expressed higher levels when compared to the control group.

The initial phase of hMSCs in vitro osteogenic differentiation

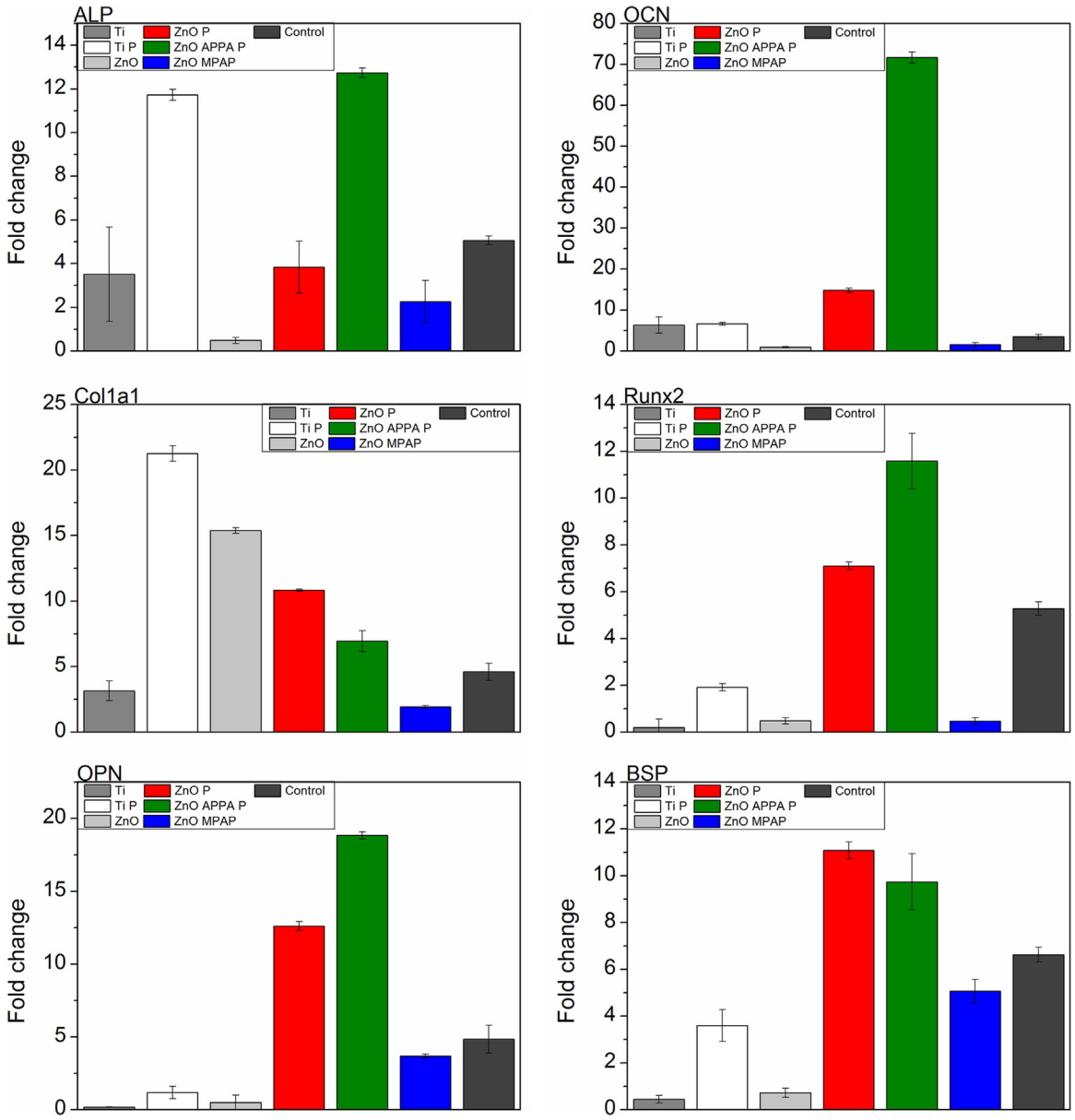

Fig. 7. Osteogenic expression of target genes measured by real-time quantitative RT-PCR quantified during hMSCs culture onto control and bio-functionalized samples at day 7. Expression levels are expressed as fold change of those measured during hMSCs culture in osteogenic and non-osteogenic media.

consists of an increase in the number of cells from day 1–4 [37]. Human mesenchymal stem cells have been shown to differentiate into osteoblast-like cells after 5–14 days exposure to osteogenic medium [37,38], being considered as hMSC-derived osteoblasts. This stage is characterized by the transcription and protein expression of ALP [39], and Runx2 [40,41]. After this initial peak of ALP and Runx2, their level starts to decline and the final stage (14–28 days) consists in a high expression of OCN and OPN, followed by calcium phosphate mineral deposition [37]. However, the differentiation of hMSCs in vitro largely depends on the culture conditions, biochemical environment and mechanical factors [42]. In this way, the difference in the surface chemistry of ZnO thin films samples might have influenced the differentiation process of hMSCs. This surface chemistry effect can be detected by the increased OCN expression at 7 days of culture for ZnO APPA P, indicating the presence of differentiated osteoblasts.

Furthermore, it can be noticed that all the genes that indicate osteogenic differentiation (OCN, OPN, and BSP) were up-regulated for ZnO APPA P sample. OCN is the most specific gene for mineralization in differentiated osteoblasts and showed a dramatic increase in the ZnO APPA P sample (> 70), indicating a rapid induction of cellular differentiation [43]. Only the Col1a1 gene presented a lower expression for ZnO APPA P (< 9). However, Col1a1 is considered an early marker for osteogenic differentiation and is not highly expressed in terminally differentiated osteoblasts [44]. This indicates that at day 7 the hMSCs were completely differentiated to osteoblasts for ZnO APPA P sample. This result is consistent with the lower proliferation rate on day 5 in MTS assay for the hMSCs cultured upon ZnO APPA P sample.

3.4. Calcium phosphate nucleation by DMP1 peptides

The in vitro mineralization assay was performed to analyze the formation of calcium phosphate biominerals by DMP1 peptides without the presence of hMSCs. In general, the presence of the peptides led to the formation of minerals with a needle- and plate-like morphology, as shown in Fig. 8. This indicates apatite crystal growth takes place via octacalcium phosphate ($Ca_8(HPO_4)_2(PO_4)_4{\cdot}5H_2O$) as an intermediate for hydroxyapatite ($Ca_{10}(PO_4)_6(OH)_2$). Even under ideal hydroxyapatite precipitation conditions, the precipitates are generally

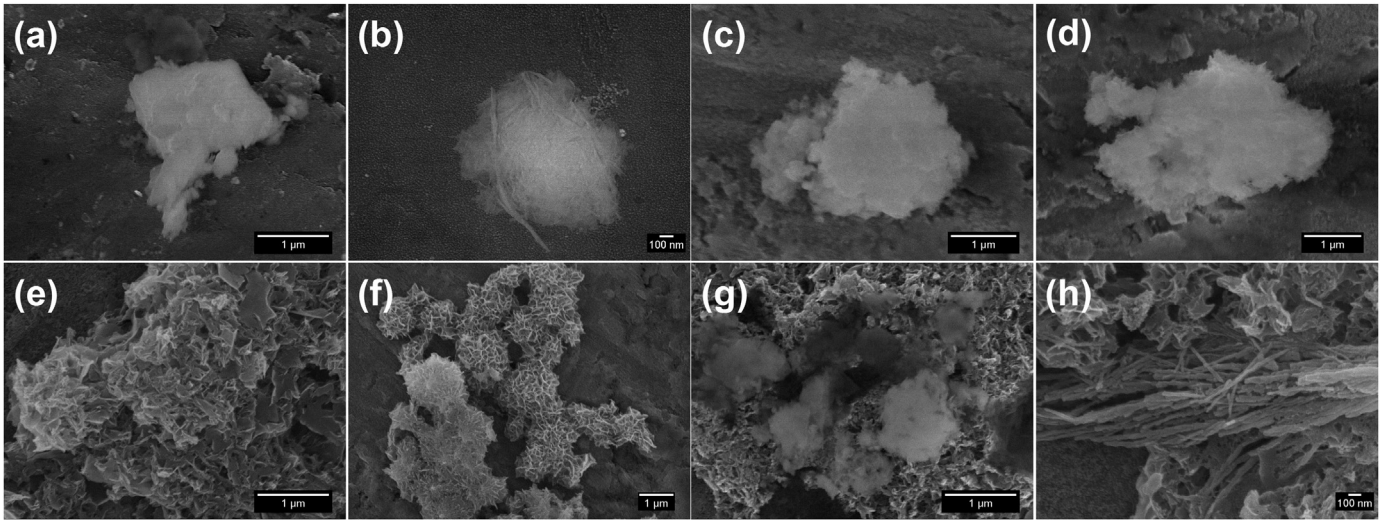

Fig. 8. SEM images from the in vitro mineralization for the different samples: Ti (a), Ti P (b) ZnO (c), ZnO P (d), ZnO APPA (e), ZnO APPA P (f), ZnO MPA (g) and ZnO MPA P (h). In general, the presence of the peptides led to the formation of minerals with a needle- and plate-like morphology, indicating apatite crystal growth via octacalcium phosphate ($Ca_8(HPO_4)_2(PO_4)_4{\cdot}5H_2O$) as an intermediate.

Table 1
Calcium and phosphorus molar ratio analyzed by EDS for the bio-functionalized samples.

Sample	Ca/P molar ratio
Ti P	3.70 (± 0.01)
ZnO P	1.02 (± 0.03)
ZnO APPA P	1.25 (± 0.03)
ZnO MPA P	1.30 (± 0.02)

nonstoichiometric, suggesting the formation of calcium-deficient apatites [45]. Similar to hydroxyapatite, octacalcium phosphate plays an important role in the in vivo formation of apatitic biominerals, participating in the initial phase of enamel and bone formation [46]. In order to confirm the type of calcium phosphate mineral formed, the Ca/P molar ratio was analyzed by EDS for the bio-functionalized samples, as shown in Table 1. The EDS analysis indicated that the Ca/P molar ratio was consistent with the atomic ratio for calcium orthophosphate minerals [47]. The samples ZnO APPA P and ZnO MPA P showed a Ca/P molar ratio closer to that of octacalcium phosphate, which is 1.33 [48].

3.5. Corrosion resistance of bio-functionalized materials

The electrochemical behavior of the samples was analyzed in terms of corrosion resistance. Only the results for bio-functionalized surfaces are shown, once the corrosion resistance behavior of the control samples (Ti and ZnO) were previously reported in our work [10]. The open circuit potentials (E_{OCP}) results acquired from the bio-functionalized ZnO thin films are presented in Fig. 9. In general, the stability of E_{OCP} in function of time indicates that no significant change occurred on the surface under these exposure conditions. The E_{OCP} of ZnO P (-0.12 V) and ZnO APPA P (-0.13 V) samples are more positive than that of Ti P (-0.18 V) and ZnO MPA P (-0.22 V). Furthermore, a shift to noble potentials for the bio-functionalized samples was observed when compared to the controls Ti (-0.55 V) and ZnO (-0.23 V) samples, as previously reported [10]. This suggests a higher corrosion resistance for ZnO P and ZnO APPA P samples, once the more positive is the E_{OCP} the lower is the corrosion tendency [49]. The DMP1 peptides can provide a protection by preventing corrosive ions from approaching the surface [18]. However, defects on the surface may lead to the degradation of the organic material due to water transport through the coating

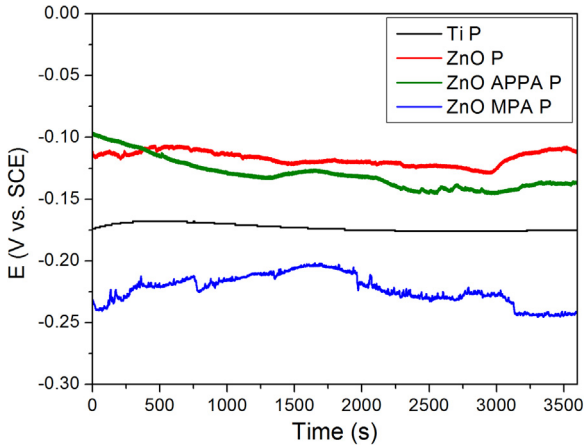

Fig. 9. Open circuit potentials vs time obtained from the bio-functionalized ZnO thin films. A more positive E_{OCP} value indicated higher corrosion resistance for ZnO P and ZnO APPA P samples.

[50,51]. In this way, the presence of defects may cause the material corrosion. This effect is probably observed for Ti P and ZnO MPA P samples, which displayed a more negative potential.

From the Bode plot, Fig. 10a, it was possible to determine the impedance module (|Z|) and capacitance from the bio-functionalized samples. The resistance of all the system presented by |Z| values considering the frequency of 0.05 Hz is in the following order from greatest to smallest: ZnO P ($8.01 \times 10^4\ \Omega\,cm^2$) > ZnO APPA P ($6.10 \times 10^4\ \Omega\,cm^2$) > ZnO MPA P ($3.50 \times 10^4\ \Omega\,cm^2$) > Ti P ($1.24 \times 10^4\ \Omega\,cm^2$). As higher the |Z| at low frequencies, lower is the corrosion tendency [52]. This indicates that ZnO P and ZnO APPA P showed increased corrosion resistance. As the frequency increases, a decrease in the resistance of the system is detected indicating the capacitive nature of the bio-functionalized samples [49]. The phase angle plots for all samples are shown in Fig. 10b. Capacitive behavior at low frequencies (< 10 Hz) with a phase angle > 80° was observed for Ti P sample, while a low capacitive behavior within high frequencies (> 1k Hz) was detected. However, for ZnO P, ZnO APPA P and ZnO MPA P sample the initial phase angle at low frequencies was smaller along with significantly high total resistance presented than that of the Ti P group. In this way, it is clear that the bio-functionalized ZnO thin films present lower capacitive and higher resistive behavior, meaning better corrosion

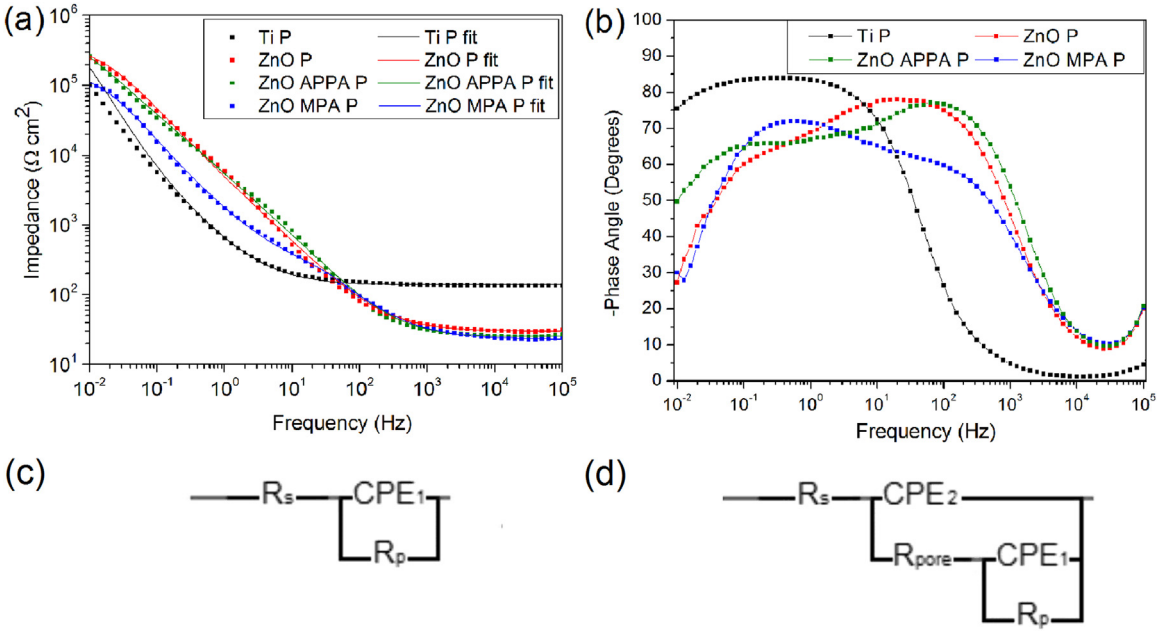

Fig. 10. Bode plots (a) and impedance phase angle plots (b) for the bio-functionalized surfaces. Equivalent circuits proposed to the experimental data based on EIS behavior: with one time constant for Ti P (c) and with two-time constants for ZnO P, ZnO APPA P, and ZnO MPA P (d). The bio-functionalized ZnO thin films presented better corrosion resistance tendency.

resistance tendency caused by the presence of the oxide thin film. The fitting for phase angle plots based on equivalent circuit models is shown in Fig S7-S10.

Equivalent circuit models for Ti P (Fig. 10c), ZnO P, ZnO APPA P, and ZnO MPA P (Fig. 10d) samples were used to analyze EIS data. Once the fittings were consistent with EIS data, the equivalent circuit models proposed are reliable. A constant phase element (CPE) was used instead of a pure capacitor due to the non-ideal behavior associated with the experimental conditions [53]. A small and similar resistance of the electrolyte solution, represented by R_s, was observed in all the EIS tests. The Ti P sample was represented by a modified Randle's circuit with a CPE, once it shows only one time constant in phase angle plot. The samples ZnO P, ZnO APPA P, and ZnO MPA P were represented by an equivalent circuit containing two cascaded CPE, meaning an inner layer (R_p and CPE_1) and an outer porous layer (R_{pore} and CPE_2). The resistances of the inner barrier and outer porous layers are represented by the notations R_p and R_{pore}, respectively.

The electrochemical parameters obtained from the fitting procedures are summarized in Table 2. The parameter R_p is important in the assessment of the working electrode corrosion resistance, it is associated to the contributions of the charge-transfer resistances, the oxide thin film resistance, and the migration of point defects mediated metal dissolution [54]. From Table 2 it was possible to observe that the R_p values were at least two orders of magnitude higher when compared to the R_{pore}, indicating a higher corrosion resistance provided by the inner layer R_p. Moreover, the bio-functionalized ZnO thin films presented a higher R_p value when compared to the Ti P sample. This result suggested that the presence of the oxide in combination with the DMP1 peptides acted inhibiting charge transfer at substrate/electrolyte interface, reducing metallic ions release, and consequently enhancing the corrosion resistance [52].

The electrochemical behavior of the bio-functionalized samples was analyzed through Tafel extrapolation from potentiodynamic polarization data by estimating corrosion potential (E_{corr}) and corrosion current density (I_{corr}). In terms of E_{corr}, Fig. 11a, the results indicated that no significant changes were observed for the bio-functionalized samples. However, when compared to pristine Ti (-0.63 V) [10], the corrosion potentials of bio-functionalized ZnO thin films samples shifted positively indicating a suppression of Ti dissolution caused by the protective nature of the ZnO thin film and the DMP1 peptides. The most positive E_{corr} value (-0.46 V) was observed for ZnO APPA P sample. A significant decrease in I_{corr} value is shown in Fig. 11b for ZnO APPA P sample (8.91×10^{-7} A/cm^2), supporting the idea of lower corrosion tendency for this sample. A possible explanation for this phenomenon may be related with the strong interaction between the ZnO thin film surface, the APPA molecule, and the DMP1 peptides, providing a better barrier protection for ZnO APPA P sample that prevents corrosion. On the other hand, an increase in I_{corr} value (3.05×10^{-6} A/cm^2) was observed for

Table 2
Electrochemical parameters obtained from equivalent circuit modeling determined from Fig. 10 (c-d) with standard deviations for the analyzed samples.

Sample	Parameters							
	R_s (Ω/cm^2)	R_p (Ω/cm^2)	CPE_1 (Ω^{-1} S^n cm^{-2})	n_1	R_{pore} (Ω/cm^2)	CPE_2 (Ω^{-1} S^n cm^{-2})	n_2	χ^2
Ti P	20.4 (± 5.78)	1.00×10^4 (± 184)	3.11×10^{-4} (± 0.25)	0.944 (± 0.07)	–	–	–	3.16×10^{-3} (± 0.79)
ZnO P	30.1 (± 4.31)	4.05×10^5 (± 147)	1.19×10^{-5} (± 0.16)	0.757 (± 0.09)	1.56×10^1 (± 2.43)	$2.66\ 10^{-6}$ (± 0.31)	0.990 (± 0.06)	6.62×10^{-3} (± 0.14)
ZnO APPA P	25.2 (± 4.44)	1.00×10^6 (± 43.9)	1.40×10^{-5} (± 0.80)	0.703 (± 0.04)	2.01×10^1 (± 2.91)	2.63×10^{-6} (± 0.33)	0.995 (± 0.03)	7.46×10^{-3} (± 0.65)
ZnO MPA P	23.0 (± 4.89)	1.64×10^5 (± 20.9)	8.74×10^{-4} (± 0.17)	0.926 (± 0.05)	1.59×10^3 (± 4.78)	2.93×10^{-5} (± 0.66)	0.800 (± 0.08)	5.88×10^{-3} (± 0.07)

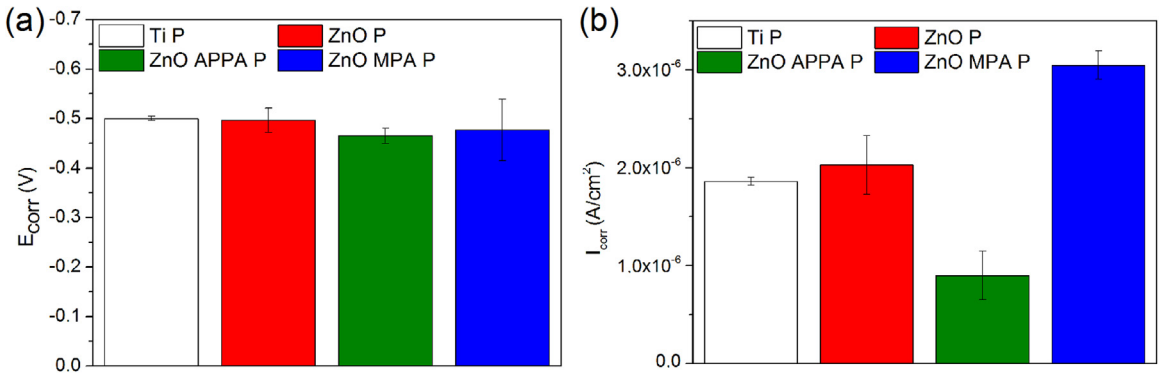

Fig. 11. Corrosion potential, E_{corr} (a) and corrosion current density, I_{corr} (b) are shown for all bio-functionalized ZnO thin films. No significant changes in the E_{corr} values were observed for the bio-functionalized samples. A significant decrease in I_{corr} value was observed for ZnO APPA P sample, indicating a lower corrosion tendency.

ZnO MPA P sample, indicating a higher corrosion rate. It can be related to the presence of defects on the surface that increases the corrosion. Besides that, different combinations of biomolecules and metals may present different ranges of effects [55].

4. Conclusions

In summary, this work describes the bio-functionalization of ZnO thin films with DMP1 peptides to improve the physicochemical, osteogenic and corrosion properties of this material for use in implants application. ZnO thin films were synthesized by sol-gel route and two different bifunctional molecules, APPA and MPA, were used for better immobilization of DMP1 peptides on the oxide surface. The bio-functionalization was confirmed by the presence of amine groups detected with ATR-FTIR and XPS. From ATR-FTIR, a characteristic band at 1536 cm^{-1} was attributed to -NH_2 groups from peptides or amino acids. By the XPS results two contributions were observed for N1s spectra: the main component (N1) related to the amide groups in the peptide backbones and amine groups on the side chains; and an N2 contribution consistent with amide groups that were strongly interacting with inorganic substrates. Moreover, through the surface characterization, it was observed that there was an increase in wettability, surface energy, and a homogeneous coverage of the peptides in ZnO APPA P and ZnO MPA P samples, associated with the presence of the terminal functional groups -NH_2 and -COOH from these samples. Regarding the biocompatibility, the bio-functionalized samples showed the capability of modulating hMSCs coating the surface with high affinity and proliferation in a preliminary in vitro study. Furthermore, all the genes associated with later stages of osteogenic differentiation (OCN, OPN, and BSP) were up-regulated for ZnO APPA P on day 7, indicating that this sample stimulated osteoblastic differentiation from hMSCs. A dramatic increase in the OCN gene expression (> 70) was observed for ZnO APPA P, indicating a rapid induction of hMSCs differentiation into osteoblasts. Additionally, ZnO APPA P and ZnO MPA P showed a Ca/P ratio of 1.25 and 1.30, respectively. This ratio indicated formation of octacalcium phosphate (1.33), an apatitic biomineral that is formed in the initial phase of enamel and bone development. Electrochemical results indicated that bio-functionalized ZnO thin films presented noble E_{OCP}, EIS, I_{corr}, and E_{corr} values associated with increased corrosion resistance. More specifically, noble E_{OCP} (-0.13 V), E_{corr} (-0.46 V), and I_{corr} (8.91×10^{-7} A/cm^2) values were observed for ZnO APPA P sample. Therefore, in summary the results obtained for ZnO APPA P, showed enhanced osteogenic, apatite nucleation, and better corrosion resistance properties indicating promising applications in biomedical devices.

Acknowledgments

The authors acknowledge Dr. Elidiane C. Rangel, Dr. Marcelo Orlandi, Dr. Valmor R. Mastelaro, and Dr. Carlos F. O. Graeff for the contact angle, SEM, XPS, and corrosion measurements, respectively. This work was financially supported by São Paulo Research Foundation (FAPESP, grants 2013/07296-2; 2013/09963-6; 2014/01713-3; 2014/27015-0; 2017/15035-5), NIH grant DE 11657 and the Brodie Endowment Fund.

Appendix A. Supporting information

Supplementary data associated with this article can be found in the online version at doi:10.1016/j.ceramint.2018.08.136.

References

[1] S.A. Alves, A.L. Rossi, A.R. Ribeiro, J. Werckmann, J.-P. Celis, L.A. Rocha, T. Shokuhfar, A first insight on the bio-functionalization mechanisms of TiO2 nanotubes with calcium, phosphorous and zinc by reverse polarization anodization, Surf. Coat. Technol. 324 (2017) 153–166.
[2] L. Levin, Dealing with dental implant failures, J. Appl. Oral. Sci. 16 (2008) 171–175.
[3] F. Javed, H. Malmstrom, S.V. Kellesarian, A.A. Al-Kheraif, F. Vohra, G.E. Romanos, Efficacy of Vitamin D3 Supplementation on Osseointegration of Implants, Implant Dent. 25 (2016) 281–287.
[4] J.-J. Ryu, K. Park, H.-S. Kim, C.-M. Jeong, J.-B. Huh, Effects of anodized titanium with Arg-Gly-Asp (RGD) peptide immobilized via chemical grafting or physical adsorption on bone cell adhesion and differentiation, Int. J. Oral. Maxillofac. Implants 28 (2013) 963–972.
[5] M. Razavi, M. Fathi, O. Savabi, D. Vashaee, L. Tayebi, In vivo study of nanostructured akermanite/PEO coating on biodegradable magnesium alloy for biomedical applications, J. Biomed. Mater. Res. A. 103 (2015) 1798–1808.
[6] A. Civantos, E. Martínez-Campos, V. Ramos, C. Elvira, A. Gallardo, A. Abarrategi, Titanium Coatings and Surface Modifications: toward Clinically Useful Bioactive Implants, ACS Biomater. Sci. Eng. 3 (2017) 1245–1261.
[7] A. Sirelkhatim, S. Mahmud, A. Seeni, N.H.M. Kaus, L.C. Ann, S.K.M. Bakhori, H. Hasan, D. Mohamad, Review on zinc oxide nanoparticles: antibacterial activity and toxicity mechanism, Nano-Micro Lett. 7 (2015) 219–242.
[8] G. Colon, B.C. Ward, T.J. Webster, Increased osteoblast and decreased Staphylococcus epidermidis functions on nanophase ZnO and TiO2, J. Biomed. Mater. Res. A. 78A (2006) 595–604.
[9] W. Wang, T.L. Li, H.M. Wong, P.K. Chu, R.Y.T. Kao, S. Wu, F.K.L. Leung, T.M. Wong, M.K.T. To, K.M.C. Cheung, K.W.K. Yeung, Development of novel implants with self-antibacterial performance through in-situ growth of 1D ZnO nanowire, Colloids Surf. B Biointerfaces 141 (2016) 623–633.
[10] L.D. Trino, L.F.G. Dias, L.G.S. Albano, E.S. Bronze-Uhle, E.C. Rangel, C.F.O. Graeff, P.N. Lisboa-Filho, Zinc oxide surface functionalization and related effects on corrosion resistance of titanium implants, Ceram. Int. 44 (2018) 4000–4008.
[11] D. Bian, Y. Guo, Y. Zhao, Influence of zinc oxide on corrosion resistance of alumina based chemically bonded ceramic coatings, Russ. J. Appl. Chem. 89 (2016) 2091–2094.
[12] E. G-Berasategui, R. Bayón, C. Zubizarreta, J. Barriga, R. Barros, R. Martins, E. Fortunato, Corrosion resistance analysis of aluminium-doped zinc oxide layers deposited by pulsed magnetron sputtering (Part B), Thin Solid Films. 594 (2015) 256–260.
[13] S.Z. Khalajabadi, M.R. Abdul Kadir, S. Izman, A. Samavati, Z. Othaman, Synthesis,

microstructure and biodegradation behavior of nano-Si and nano-ZnO/Si coatings on a Mg/HA/TiO2/MgO nanocomposite, Ceram. Int. 41 (2015) 11346–11358.
[14] A.M. Vilardell, N. Cinca, N. Garcia-Giralt, S. Dosta, I.G. Cano, X. Nogués, J.M. Guilemany, Osteoblastic cell response on high-rough titanium coatings by cold spray, J. Mater. Sci. Mater. Med. 29 (2018) 19.
[15] J.D. Padovano, S. Ravindran, P.T. Snee, A. Ramachandran, A.K. Bedran-Russo, A. George, DMP1-derived peptides promote remineralization of human dentin, J. Dent. Res. 94 (2015) 608–614.
[16] G. He, T. Dahl, A. Veis, A. George, Nucleation of apatite crystals in vitro by self-assembled dentin matrix protein 1, Nat. Mater. 2 (2003) 552–558.
[17] V. Uskokovic, D.P. Uskokovic, Nanotechnologies in Preventive and Regenerative Medicine, first ed., Elsevier, 2017.
[18] L.D. Trino, E.S. Bronze-Uhle, A. Ramachandran, P.N. Lisboa-Filho, M.T. Mathew, A. George, Titanium surface bio-functionalization using osteogenic peptides: surface chemistry, biocompatibility, corrosion and tribocorrosion aspects, J. Mech. Behav. Biomed. Mater. 81 (2018) 26–38.
[19] S. Ravindran, Q. Gao, M. Kotecha, R.L. Magin, S. Karol, A. Bedran-Russo, A. George, Biomimetic extracellular matrix-incorporated scaffold induces osteogenic gene expression in human marrow stromal cells, Tissue Eng. Part A. 18 (2012) 295–309.
[20] M.S. Cintrón, D.J. Hinchliffe, FT-IR examination of the development of secondary cell wall in cotton fibers, Fibers 3 (2015) 30–40.
[21] X. Wang, J. Liu, X. Huang, L. Men, M. Guo, D. Sun, Controlled synthesis of linear polyaniline tubes and dendritic polyaniline fibers with stearic acid, Polym. Bull. 60 (2008) 1–6.
[22] N. Abidi, E. Hequet, L. Cabrales, J. Gannaway, T. Wilkins, L.W. Wells, Evaluating cell wall structure and composition of developing cotton fibers using Fourier transform infrared spectroscopy and thermogravimetric analysis, J. Appl. Polym. Sci. 107 (2008) 476–486.
[23] K. Nakamoto, Infrared and Raman Spectra of Inorganic and Coordination Compounds, sixth ed., John Wiley & Sons Inc, 2008.
[24] Y. Zhu, A. Apostoluk, P. Gautier, A. Valette, L. Omar, T. Cornier, J.M. Bluet, K. Masenelli-Varlot, S. Daniele, B. Masenelli, Intense visible emission from ZnO/PAAX (X = H or Na) nanocomposite synthesized via a simple and scalable sol-gel method, Sci. Rep. 6 (2016) 1–11.
[25] K.P. Fears, D.Y. Petrovykh, T.D. Clark, Evaluating protocols and analytical methods for peptide adsorption experiments, Biointerphases 8 (2013) 20.
[26] J.S. Stevens, A.C. de Luca, M. Pelendritis, G. Terenghi, S. Downes, S.L.M. Schroeder, Quantitative analysis of complex amino acids and RGD peptides by X-ray photoelectron spectroscopy (XPS), Surf. Interface Anal. 45 (2013) 1238–1246.
[27] S. Jewett, D. Zemlyanov, A. Ivanisevic, Adsorption of mixed peptide/thiol adlayers on InAs: assessment of different functionalization strategies using X-ray photoelectron spectroscopy, J. Phys. Chem. C. 115 (2011) 14244–14252.
[28] M. Shaban, M. Zayed, H. Hamdy, Nanostructured ZnO thin films for self-cleaning applications, RSC Adv. 7 (2017) 617–631.
[29] K.E. Sapsford, W.R. Algar, L. Berti, K.B. Gemmill, B.J. Casey, E. Oh, M.H. Stewart, I.L. Medintz, Functionalizing nanoparticles with biological molecules: developing chemistries that facilitate nanotechnology, Chem. Rev. 113 (2013) 1904–2074.
[30] M. Rabe, D. Verdes, S. Seeger, Understanding protein adsorption phenomena at solid surfaces, Adv. Colloid Interface Sci. 162 (2011) 87–106.
[31] W.J. Choi, J. Jung, S. Lee, Y.J. Chung, C.-S. Yang, Y.K. Lee, Y.-S. Lee, J.K. Park, H.W. Ko, J.-O. Lee, Effects of substrate conductivity on cell morphogenesis and proliferation using tailored, atomic layer deposition-grown ZnO thin films, Sci. Rep. 5 (2015) 9974.
[32] A. Ahmad Khalili, M.R. Ahmad, A review of cell adhesion studies for biomedical and biological applications, Int. J. Mol. Sci. 16 (2015) 18149–18184.
[33] Y. Wang, F. Huang, D. Pan, B. Li, D. Chen, W. Lin, X. Chen, R. Li, Z. Lin, Ultraviolet-light-induced bactericidal mechanism on ZnO single crystals, Chem. Commun. (2009) 6783–6785.
[34] J.-B. Park, Effects of 17-α ethynyl estradiol on proliferation, differentiation & mineralization of osteoprecursor cells, Indian J. Med. Res. 136 (2012) 466–470.
[35] M. Khacho, R.S. Slack, Mitochondrial activity in the regulation of stem cell self-renewal and differentiation, Curr. Opin. Cell Biol. 49 (2017) 1–8.
[36] E. Esen, F. Long, Aerobic glycolysis in osteoblasts, Curr. Osteoporos. Rep. 12 (2014) 433–438.
[37] Z. Huang, E.R. Nelson, R.L. Smith, S.B. Goodman, The sequential expression profiles of growth factors from osteoprogenitors [correction of osteroprogenitors] to osteoblasts in vitro, Tissue Eng. 13 (2007) 2311–2320.
[38] A.I. Caplan, The mesengenic process, Clin. Plast. Surg. 21 (1994) 429–435.
[39] J.E. Aubin, Regulation of osteoblast formation and function, Rev. Endocr. Metab. Disord. 2 (2001) 81–94.
[40] Q. Chen, P. Shou, C. Zheng, M. Jiang, G. Cao, Q. Yang, J. Cao, N. Xie, T. Velletri, X. Zhang, C. Xu, L. Zhang, H. Yang, J. Hou, Y. Wang, Y. Shi, Fate decision of mesenchymal stem cells: adipocytes or osteoblasts? Cell Death Differ. 23 (2016) 1128–1139.
[41] M. Fakhry, E. Hamade, B. Badran, R. Buchet, D. Magne, Molecular mechanisms of mesenchymal stem cell differentiation towards osteoblasts, World J. Stem Cells 5 (2013) 136–148.
[42] E. Birmingham, G.L. Niebur, P.E. McHugh, G. Shaw, F.P. Barry, L.M. McNamara, Osteogenic differentiation of mesenchymal stem cells is regulated by osteocyte and osteoblast cells in a simplified bone niche, Eur. Cell. Mater. 23 (2012) 13–27.
[43] C. Zheng, J. Wang, Y. Liu, Q. Yu, Y. Liu, N. Deng, J. Liu, Functional selenium nanoparticles enhanced stem cell osteoblastic differentiation through BMP signaling pathways, Adv. Funct. Mater. 24 (2014) 6872–6883.
[44] L. Shi, F. Wang, W. Zhu, Z. Xu, S. Fuchs, J. Hilborn, L. Zhu, Q. Ma, Y. Wang, X. Weng, D.A. Ossipov, Self-healing silk fibroin-based hydrogel for bone regeneration: dynamic metal-ligand self-assembly approach, Adv. Funct. Mater. 27 (2017).
[45] L. Wang, G.H. Nancollas, Calcium orthophosphates: crystallization and dissolution, Chem. Rev. 108 (2008) 4628–4669.
[46] N. Eliaz, N. Metoki, Calcium phosphate bioceramics: a review of their history, structure, properties, coating technologies and biomedical applications, Mater. Basel Switz. 10 (2017).
[47] S.V. Dorozhkin, Calcium orthophosphates, Biomatter 1 (2011) 121–164.
[48] Maria Canillas, Pilar Pena, Antonio, H. de Aza Miguel, A. Rodríguez, Calcium phosphates for biomedical applications, Bol. Soc. Esp. Cerámica Vidr. 56 (2017) 91–112.
[49] J. Grotberg, A. Hamlekhan, A. Butt, S. Patel, D. Royhman, T. Shokuhfar, C. Sukotjo, C. Takoudis, M.T. Mathew, Thermally oxidized titania nanotubes enhance the corrosion resistance of Ti6Al4V, Mater. Sci. Eng. C. 59 (2016) 677–689.
[50] R.G. Kelly, J.R. Scully, D. Shoesmith, R.G. Buchheit, Electrochemical Techniques in Corrosion Science and Engineering, CRC Press, 2002.
[51] R.J.K. Wood, 2.15 - Tribocorrosion A2 - Cottis, Bob, in: M. Graham, R. Lindsay, S. Lyon, T. Richardson, D. Scantlebury, H. Stott (Eds.), Shreirs Corros. Elsevier, Oxford, 2010, pp. 1005–1050.
[52] X. Zhang, H. Wang, J. Li, X. He, R. Hang, X. Huang, L. Tian, B. Tang, Corrosion behavior of Zn-incorporated antibacterial TiO2 porous coating on titanium, Ceram. Int. 42 (2016) 17095–17100.
[53] L. Liu, J. Xu, P. Munroe, J. Xu, Z. Xie, Electrochemical behavior of (Ti1 − xNbx)5Si3 nanocrystalline films in simulated physiological media, Acta Biomater. 10 (2014) 1005–1013.
[54] H. Krawiec, V. Vignal, E. Schwarzenboeck, J. Banas, Role of plastic deformation and microstructure in the micro-electrochemical behaviour of Ti–6Al–4V in sodium chloride solution, Electrochim. Acta 104 (2013) 400–406.
[55] D. Royhman, R. Radhakrishnan, J.C.-C. Yuan, M.T. Mathew, L.G. Mercuri, C. Sukotjo, An electrochemical investigation of TMJ implant metal alloys in an artificial joint fluid environment: the influence of pH variation, J. Cranio-Maxillo-Fac. Surg. Off. Publ. Eur. Assoc. Cranio-Maxillo-Fac. Surg. 42 (2014) 1052–1061.